



Selective excitation of plasmon resonances with single V-point cylindrical vector beams

BO XU,¹ BRENDAN M. HEFFERNAN,¹ KYUYOUNG BAE,² MARK E. SIEMENS,³  JULIET T. GOPINATH,^{1,2,4}  AND WOUNJHANG PARK^{2,4,*} 

¹*Department of Physics, University of Colorado, Boulder, Colorado 80309, USA*

²*Department of Electrical, Computer, and Energy Engineering, University of Colorado, Boulder, Colorado 80309, USA*

³*Department of Physics and Astronomy, University of Denver, 2112 East Wesley Avenue, Denver, Colorado 80210, USA*

⁴*Materials Science and Energy Engineering, University of Colorado, Boulder, CO 80309, USA*

*won.park@colorado.edu

Abstract: We use a rigorous group theoretical method to identify a class of cylindrical vector beams that can selectively excite the plasmon modes of axially symmetric plasmonic structures. Our choice of the single V-point cylindrical vector beams as the basis to decompose cylindrical beams dramatically simplifies the symmetry analysis in the group theory framework. With numerical simulations, we demonstrate that any plasmon eigenmodes, bright or dark, can be selectively excited individually or jointly. A straightforward protocol to get access to the desired plasmon mode using symmetry coupling is presented.

© 2021 Optical Society of America under the terms of the [OSA Open Access Publishing Agreement](#)

1. Introduction

The localized surface plasmon resonance (LSPR) of a metallic nanostructure offers strong near-field enhancement and far-field scattering, leading to a diversity of applications such as enhanced chemical and biological sensors [1,2], fluorescence enhancement [3], surface-enhanced Raman scattering [4], second harmonic generation [5], plasmon-enhanced photovoltaics [6,7] and photocatalysis [8]. To continue and accelerate future progress, it is important to gain access to all plasmon modes supported by a nanostructure. When a nanostructure interacts with a plane wave or a Gaussian beam, the LSPR modes which can be excited is highly dependent on the nanostructure's size. In the long wavelength limit where the nanostructure is much smaller than the wavelength of the electromagnetic wave, all free electrons on the nanostructure roughly experience the same phase of the incident field, which results in dipole LSPRs. As the size increases, the phase retardation over the nanostructure can lead to non-dipolar multipole LSPRs, also known as dark plasmons. Due to the vanishing of dipole moment, dark plasmons usually radiate much less energy into the far-field than dipole plasmons and exhibit much stronger near-field enhancements and longer lifetimes [9]. The coupling of a narrow and dark mode with broad and bright dipole modes can also lead to plasmonic Fano resonances [10]. Therefore, dark plasmons offer great opportunities for novel plasmonic applications.

Past work on selectively exciting dark plasmon modes has focused on using cylindrical vector (CV) beams [9,11–14] and circularly polarized Laguerre–Gaussian beams [15–19]. Compared to a plane wave which has homogenous polarization and phase distribution over the beam cross section, a CV beam has a spatially varying polarization distribution and a circularly polarized Laguerre–Gaussian beam has a spatially varying phase distribution. If a beam's polarization or phase distribution pattern matches with that of a dark mode LSPR, the light can couple to the LSPR, exciting that dark mode LSPR. The most commonly used CV beams in the past research are the azimuthally polarized and radially polarized beams due to their simple but unique

polarization distribution. It has been demonstrated that tightly focused azimuthally and radially polarized beams can couple into small metallic nanoparticle oligomers [11–13] and excite dark plasmon resonances which cannot be excited by plane waves. Tightly focused radially polarized beams have also been experimentally demonstrated to selectively excite a three-dimensionally oriented plasmonic dipole mode in a metallic nanosphere [14]. Meanwhile, focused circularly polarized Laguerre–Gaussian beams with well-defined orbital angular momentum have been used to selectively excite multipole resonance modes in metallic nanodisks [15], nanodisk oligomers [16], highly symmetrical antenna arrays [17–19], and dielectric spheres [20].

Sancho-Parramon et al. [11] suggested that symmetry is related to the selective and exclusive excitations, but the discussion was limited to a few special structures under illumination by azimuthally polarized or radially polarized beams. In this paper, we identify an orthonormal mode basis set for CV beams that has a one-to-one correspondence with the plasmon modes of any axially symmetric plasmonic structure. They allow a rigorous and concise group theoretical analysis and enables true single-mode excitation. We refer to this cylindrically symmetric orthonormal mode basis as single V-point (SV) cylindrical vector beams, or SV beams, in the rest of the paper. SV beams are a set of special cases of Poincaré beams [21,22] composed of two conjugated Laguerre–Gaussian modes. That is, an SV beam is a combination of two Laguerre-Gaussian beams with orthogonal polarizations whose radial parameters are identical, but the azimuthal parameters have opposite signs. SV beams are known for their “flower” and “spider-web” shaped polarization patterns [23,24] which exhibit rich symmetry properties. Figure 1 illustrates the field patterns of azimuthally polarized or radially polarized beams and two examples of SV beams.

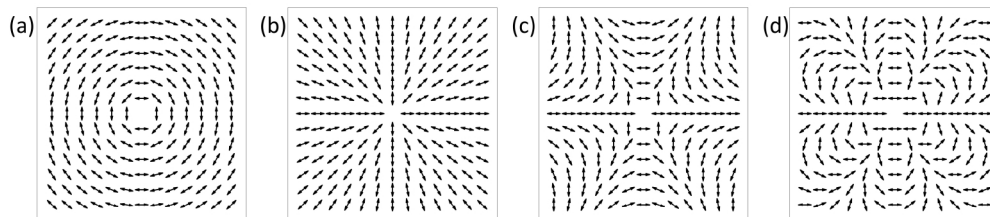


Fig. 1. Time independent polarization distribution of (a) azimuthally polarized beam, (b) radially polarized beam, (c) a single V-point cylindrical vector (SV) beam with azimuthal parameter $l = 2$ which has a “spider-web” shaped pattern, and (d) an SV beam with azimuthal parameter $l = -4$ which has a “flower” shaped pattern.

Unlike circularly polarized Laguerre–Gaussian beams which have no reflection symmetry in the planes containing the beam’s symmetry axis except for a few special cases, all SV beams have reflection symmetry in multiple planes containing the beam’s symmetry axis as well as many rotational symmetry elements which can be easily spotted in their polarization distribution. Thus, SV beams are naturally more compatible with axially symmetric plasmonic structures and can be readily classified as the basis functions for the irreducible representations of the same symmetry point group as the plasmonic structure. In the case of tight focusing, which is often needed for efficient coupling with nanostructures, a tightly focused SV beam can always be decomposed into transverse and longitudinal components, each of which maintains one-to-one correspondence with the irreducible representations, as shown later in this paper. Since the incident beams are described by the same irreducible representation as the plasmon modes, we can readily establish the one-to-one selection rules between the plasmon modes and SV beams without performing any numerical simulations [15–19] or overlap integral calculations [16].

In this paper, we present a rigorous group theoretical approach to describe the symmetry of axially symmetric plasmon modes and tightly focused SV beams by the irreducible representations

of dihedral point groups. The one-to-one selection rules for the excitation of plasmon modes by tightly focused SV beams are deduced by simply invoking the orthogonality theorem. Several examples of the one-to-one selectivity are demonstrated with numerical simulations which clearly show the fundamental advantage of using SV beams as the incident beams for selective excitation. This paper provides a theoretical foundation for designing nanostructures that have highly selective interactions with tightly focused cylindrical vector beams and opens a door to the development of novel nanoscale optical devices and light sources.

2. Theoretical framework

2.1. Symmetrical nanostructures and point groups

Group theory has been widely used in photonic nanostructures like photonic crystals and plasmonic clusters [25,26]. For a given nanostructure, one can usually find a group of symmetry operators to fully describe its symmetry properties. For example, the symmetry of a sphere is described by 3D orthogonal group $O(3)$, and the symmetry of a disk is described by infinite dihedral group $D_{\infty h}$. A symmetric planar structure made of a collection of identical elements, e.g., nanospheres, can be fully described by a dihedral point group comprised of the relevant rotation and reflection operators.

For example, a planar quadrumer composed of four identical nanospheres located at the four corners of a square has the symmetry of point group D_{4h} . For each of the nanospheres, the simplest and strongest LSPR is the dipole oscillation because light couples most strongly to dipoles in the long wavelength regime. Using the dipole plasmon modes of the four individual particles, we can construct the symmetry-adapted hybridized-dipole eigenmodes of this quadrumer, as shown in Fig. 2. Each of these symmetry-adapted eigenmodes belongs to one of the irreducible representations of the D_{4h} group.

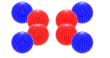
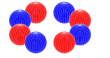
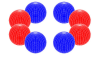
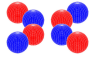
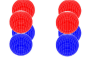
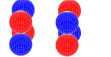
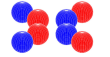
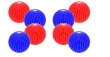
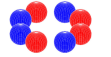
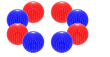
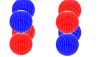
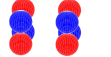
Irreducible representation	A_{1g}	A_{2g}	B_{1g}	B_{2g}	A_{2u}	B_{1u}
Hybridized-dipole plasmon mode						
Irreducible representation	E_u				E_g	
Hybridized-dipole plasmon mode						

Fig. 2. The irreducible representations of the D_{4h} group corresponding to symmetry-adapted hybridized-dipole eigenmodes of a planar quadrumer. A_{1u} and B_{2u} are not shown here because their symmetry cannot be formed by hybridization of four individual dipoles.

Each irreducible representation has a unique set of characters corresponding to the point group's symmetry operations. Therefore, we can use the projection operators to determine which of these symmetry-adapted eigenmodes belong to which irreducible representation [25]. The projection operator for irreducible representation i is defined as:

$$\hat{\Pi}_i = \frac{l_i}{h} \sum_R \chi_i(R) \cdot \hat{P}_R, \quad (1)$$

where l_i is the dimension of irreducible representation i , h is the order of the group, $\chi_i(R)$ is the character of the symmetry operation R , and \hat{P}_R is the symmetry operator corresponding to transformation R . All the needed information to construct the projection operators is listed in the point group's character table [27]. The character tables of the D_{3h} , D_{4h} and D_{6h} point groups as

the examples are presented in Supplement 1. As shown in Fig. 2, the 12 eigenmodes of hybridized dipoles are categorized into 8 irreducible representations of the D_{4h} group. If the separation between the four nanospheres in the quadrumer is large enough to neglect the interactions among them, all of the 12 plasmon modes would be degenerate in energy. For a small separation, the degeneracy will be lifted into multiple energy levels each of which can be assigned to one of the 8 irreducible representations.

The 8 irreducible representations separate the plasmon modes into in-plane and out-of-plane modes. The four linear combinations of dipole resonances that form the basis functions for the four one-dimensional representations A_{1g} , A_{2g} , B_{1g} and B_{2g} , have no net dipole moment and thus make dark plasmon modes. The other four linear combinations of the in-plane dipole modes do possess net dipole moments and belong to the two-dimensional representation E_u . The choice of basis set is not unique, and there are many ways to form a basis set for the E_u representation using linear combinations of these four dipole modes which will be introduced later. The out-of-plane dipole mode belonging to the one-dimensional representation A_{2u} possesses a net dipole moment and can be excited by plane waves at an oblique incidence. The two-dimensional out-of-plane representation E_g has a pair of quadrupole basis functions and the one-dimensional out-of-plane representation B_{1u} has the octupole basis function. As additional examples, we also summarize the eigenmodes of a planar trimer with the D_{3h} group symmetry and a planar hexamer with the D_{6h} group symmetry in Supplement 1.

2.2. Single V-point cylindrical vector beams

Cylindrical vector beams are a class of axially symmetric laser beams with spatially varying polarization, which are solutions of Maxwell's equations under the paraxial approximation [28]. In this paper, we focus on the single V-point cylindrical vector beams (SV beams) which are remarkably well-suited to be the basis functions for axial point groups' representations. First, we introduce Poincaré beams obtained by coaxial superposition of two Laguerre-Gaussian beams with orthogonal polarizations [21,22]:

$$V_{l_1, p_1, l_2, p_2} = \frac{1}{\sqrt{2}}(LG_{l_1, p_1}^+ e^{i\gamma} + LG_{l_2, p_2}^- e^{-i\gamma}). \quad (2)$$

Here $LG_{l,p}^\pm$ represents the beam profile of a Laguerre-Gaussian beam with azimuthal parameter l , radial parameter p , and circular polarization handedness \hat{e}_\pm . γ is an arbitrary relative phase of the superposition. In cylindrical coordinates (r, ϕ, z) , the beam profile $LG_{l,p}^\pm$ has a polarization handedness $\hat{e}_\pm = (\hat{r} \pm i\hat{\phi})e^{\pm i\phi}/\sqrt{2}$ and phase vortex $e^{il\phi}$. Now consider the special case of Poincaré beams with $l_1 = -l_2$, $p_1 = p_2$, and $\gamma = 0$ or $-\pi/2$. We define these beams as SV beams:

$$SV_{l,p}^\alpha = \frac{(-i)^{\frac{1-\alpha}{2}}}{\sqrt{2}}(LG_{l,p}^+ + \alpha LG_{-l,p}^-), \quad (3)$$

with parameters $\alpha = \pm 1$, $l \in \mathbb{Z}$, $p \in \mathbb{N}$.

SV beams form a complete orthonormal basis for solutions of Maxwell's equations under paraxial approximation because each pair of conjugated circularly polarized Laguerre-Gaussian beams create a pair of conjugated SV beams and vice versa. The E-field of an SV beam in cylindrical coordinates (r, ϕ, z) can be written as:

$$\begin{cases} SV_{l,p}^+ = A_{l,p}(r, z) \cdot (\hat{r}\cos[(l+1)\phi] - \hat{\phi}\sin[(l+1)\phi]) \cdot e^{i(\omega t - kz)}, \\ SV_{l,p}^- = A_{l,p}(r, z) \cdot (\hat{r}\sin[(l+1)\phi] + \hat{\phi}\cos[(l+1)\phi]) \cdot e^{i(\omega t - kz)}. \end{cases} \quad (4)$$

The amplitude scalar function [21] is:

$$A_{l,p}(r, z) = E_0 \frac{w_0}{w(z)} \left(\frac{r}{w(z)}\right)^{|l|} \exp\left(-\frac{r^2}{w^2(z)}\right) L_p^{|l|}\left(\frac{2r^2}{w^2(z)}\right) \exp\left(-ik\frac{r^2}{2R(z)} + i\psi(z)\right), \quad (5)$$

where $w(z)$ is the beam width, L_p^l is the generalized Laguerre polynomial, $R(z)$ is the wavefront curvature and $\psi(z)$ is the Gouy phase.

If $l = p = 0$, one can get the fundamental mode $SV_{0,0}^+$, x-polarized Gaussian beam, and $SV_{0,0}^-$, y-polarized Gaussian beam. But if $l \neq 0$, there is a point of polarization singularity (i.e., point of undefined polarization), which is also called a V-point [29], at $r = 0$. Thus, we refer to this set of beams as the “single V-point cylindrical vector beams” or “SV beams” because of the single V-point in the center of the beam cross section in most cases (except for $l = 0$).

As mentioned before, one key difference between the circularly polarized Laguerre–Gaussian basis and the SV basis is that the latter possesses reflection symmetries over planes containing the beam’s symmetry axis. To illustrate this point, let us consider the reflection operation in the $\phi = m\pi$ plane, $\sigma_{m\pi}$, where m is an integer. When applying the reflection to a circularly polarized Laguerre–Gaussian beam, the angular momentum of the beam flips, but SV beams are invariant under this operation:

$$\begin{cases} \hat{P}_{\sigma_{m\pi}} LG_{l,p}^+ = LG_{-l,p}^- , \\ \hat{P}_{\sigma_{m\pi}} SV_{l,p}^\alpha = SV_{l,p}^\alpha . \end{cases} \quad (6)$$

Therefore, while circularly polarized Laguerre–Gaussian beams cannot be related to dihedral point groups, SV beams are basis functions for dihedral point groups. For example, we can apply the D_{4h} group’s irreducible representation projection operators in Eq. (1) to the SV beam $SV_{1,p}^+$ and obtain

$$\hat{\Pi}_i SV_{1,p}^+ = \begin{cases} SV_{1,p}^+ , & i = B_{1g}, \\ 0 , & \text{otherwise.} \end{cases} \quad (7)$$

If we do the same for the full set of SV beams, we find that each SV beam belongs to one of the 5 in-plane irreducible representations of the D_{4h} group, and therefore can be treated as the basis functions for these representations.

Because of the polarization singularity, there’s an intensity null at the center of SV beams except for the $l = 0$ cases. For unfocused SV beams, the null might be larger than the nanostructure under study. Efficient coupling requires good spatial overlap, which in turn calls for a tight focusing the SV beams with a high numerical aperture (NA) lens. When tightly focused, the radial E-field components will contribute to both the new axial and radial E-field components, while the azimuthal E-field will simply scale in size [24]. We can separate the E-field of a focused SV beam into its transverse component $SVT_{l,p}^\alpha$ and longitudinal component $SVL_{l,p}^\alpha$.

Starting with Eq. (4), the E-field of the transverse component $SVT_{l,p}^\alpha$ can be written as:

$$\begin{cases} SVT_{l,p}^+ = (A_{l,p}^r(r, z) \cdot \hat{r} \cos[(l + 1)\phi] - A_{l,p}^\phi(r, z) \cdot \hat{\phi} \sin[(l + 1)\phi]) \cdot e^{i(\omega t - kz)}, \\ SVT_{l,p}^- = (A_{l,p}^r(r, z) \cdot \hat{r} \sin[(l + 1)\phi] + A_{l,p}^\phi(r, z) \cdot \hat{\phi} \cos[(l + 1)\phi]) \cdot e^{i(\omega t - kz)}. \end{cases} \quad (8)$$

And the longitudinal component $SVL_{l,p}^\alpha$ can be written as:

$$\begin{cases} SVL_{l,p}^+ = A_{l,p}^z(r, z) \cos[(l + 1)\phi] \hat{z} \cdot e^{i(\omega t - kz)}, \\ SVL_{l,p}^- = A_{l,p}^z(r, z) \sin[(l + 1)\phi] \hat{z} \cdot e^{i(\omega t - kz)}. \end{cases} \quad (9)$$

The new amplitude scalar functions $A_{l,p}^r, A_{l,p}^\phi, A_{l,p}^z$ can be calculated numerically through E-field vector integrals [30].

Because the two components $SVT_{l,p}^\alpha$ and $SVL_{l,p}^\alpha$ of the same tightly focused SV beam have different responses under the σ_h reflection over the $z = 0$ horizontal plane:

$$\begin{cases} \hat{P}_{\sigma_h} SVT_{l,p}^\alpha = SVT_{l,p}^\alpha, \\ \hat{P}_{\sigma_h} SVL_{l,p}^\alpha = -SVL_{l,p}^\alpha, \end{cases} \quad (10)$$

tightly focused SV beams are no longer eigenfunctions for the σ_h operator, and therefore not basis functions for any point groups which include the σ_h operator such as the D_{nh} groups. However, if we treat $SVT_{l,p}^\alpha$ and $SVL_{l,p}^\alpha$ separately, they are both eigenfunctions for the σ_h operator and still basis functions for the D_{nh} groups.

Using the D_{4h} group as an example, we apply the projection operator of each irreducible representation, as shown in Eq. (1), to the profile functions of every $SVT_{l,p}^\alpha$ and $SVL_{l,p}^\alpha$ beam component as shown in Eq. (8) and (9). The results have the same orthogonality as Eq. (7), i.e., each $SVT_{l,p}^\alpha$ and $SVL_{l,p}^\alpha$ beam component is the basis function of one of the 10 irreducible representations of the D_{4h} group. The complete results are summarized in Table 1. Based on Table 1, for the 8 one-dimensional representations (A's and B's), one can find a full set of transverse or longitudinal E-fields as the basis functions for one of these representations by $l + 1$ modulo 4. For example, any longitudinal beam component $SVL_{l,p}^+$ satisfying $\text{mod}(|l + 1|, 4) = 0$ is a basis function of A_{2u} representation. For the two-dimensional representation E_u , any pair of transverse E-field $SVT_{l,p}^\pm$ satisfying $\text{mod}(|l + 1|, 2) = 1$ can be used as a basis function pair. For example, if one chooses $SVT_{2,p}^+$ as the “x-type” basis function of E_u representation, then the “y-type” basis function is $SVT_{2,p}^-$. Similarly, for the other two-dimensional representation E_g , if one chooses $SVL_{0,p}^+$ as the “x-type” basis function, then the “y-type” basis function should be $SVL_{0,p}^-$.

Table 1. The transverse & longitudinal E-field of a tightly focused SV beam belongs to different irreducible representations of the D_{4h} group, depending on parameters l and α .

Transverse E-field $SVT_{l,p}^\alpha$	Irreducible representation	Longitudinal E-field $SVL_{l,p}^\alpha$	Irreducible representation
$\text{mod}(l + 1 , 4) = 0, \alpha = +1$	A_{1g}	$\text{mod}(l + 1 , 4) = 0, \alpha = +1$	A_{2u}
$\text{mod}(l + 1 , 4) = 0, \alpha = -1$	A_{2g}	$\text{mod}(l + 1 , 4) = 0, \alpha = -1$	A_{1u}
$\text{mod}(l + 1 , 2) = 1, \alpha = \pm 1$	E_u	$\text{mod}(l + 1 , 2) = 1, \alpha = \pm 1$	E_g
$\text{mod}(l + 1 , 4) = 2, \alpha = +1$	B_{1g}	$\text{mod}(l + 1 , 4) = 2, \alpha = +1$	B_{2u}
$\text{mod}(l + 1 , 4) = 2, \alpha = -1$	B_{2g}	$\text{mod}(l + 1 , 4) = 2, \alpha = -1$	B_{1u}

2.3. Selection rule for the coupling between the plasmon modes and SV beams

After categorizing the axially symmetric plasmonic structure's plasmon eigenmodes and the E-field of all tightly focused SV beams as the basis functions for the irreducible representations of a certain point group, we can invoke the orthogonality theorem to state the selection rule. “Two basis functions which belong either to different irreducible representations or to different columns (rows) of the same representation are orthogonal [27].” From this, we identify that only an SV beam and a plasmon mode belonging to the same irreducible representation can couple with each other. For multidimensional representations, only an SV beam and a plasmon mode belonging to the same column of the same representation can couple with each other.

We again use the D_{4h} group as an example. The radial in-phase hybridized-dipole mode, A_{1g} , shown in Fig. 2, is a basis function of the A_{1g} representation of the D_{4h} group. Thus, it is orthogonal to all SV beams except for those belonging to the same irreducible representation. That

is, only the tightly focused SV beams with SV_{lp}^+ components satisfying $\text{mod}(|l+1|, 4) = 0$ will have a non-zero overlap and can thus couple to the A_{1g} plasmon mode. Similarly, the quadrupole B_{1u} mode can only couple to the longitudinal component of tightly focused SV_{lp}^- beams satisfying $\text{mod}(|l+1|, 4) = 2$. As for the two-dimensional representations, e.g., E_u representation, the in-plane x-dipole mode and y-dipole mode are basis functions belonging to different “columns” of the same representation. Thus, the SV_{lp}^+ components with $\text{mod}(|l+1|, 2) = 1$ which are the “x-type” basis functions of E_u representation can couple to the in-plane x-dipole mode but not to the in-plane y-dipole mode. Similarly, the SV_{lp}^- components with $\text{mod}(|l+1|, 2) = 1$ which are the “y-type” basis functions of E_u representation can couple to the in-plane y-dipole mode but not to the in-plane x-dipole mode. We also tabulate the transverse and longitudinal E-fields of tightly focused SV beams as the basis functions of the irreducible representations of D_{3h} and D_{6h} point groups in [Supplement 1](#). These can be used to derive the selection rules for the plasmon modes with D_{3h} or D_{6h} symmetry.

3. Results and discussion

In order to demonstrate the selection rule, we numerically simulated interactions between tightly focused SV beam and plasmonic structures with D_{4h} symmetry using the commercial software Lumerical. To generate tightly focused SV beams, we first calculated the electromagnetic fields of circularly polarized Laguerre–Gaussian beams at the focus of a high NA objective using a multipole expansion method [20,31,32]. This method was chosen due to the common usage of multipolar fields in scattering calculations, which are a well-known basis set in spherical coordinates and solutions to Maxwell’s equations. In general, the incident beam after passing through a lens can be expressed as [33]:

$$\vec{E} \propto \sum_{j=1}^{\infty} \sum_{m_z=-j}^j g_{j,m_z}^{(m)} \vec{A}_{j,m_z}^{(m)} + g_{j,m_z}^{(e)} \vec{A}_{j,m_z}^{(e)}, \quad (11)$$

where j is the order of the multipole, $g_{j,m_z}^{(m),(e)}$ is a coefficient describing the weighting of each multipolar field, (m) , (e) describe whether the parity of the field is magnetic or electric, and $\vec{A}_{j,m_z}^{(m),(e)}$ are the multipolar fields of given order and parity [20].

After passing through the focusing element, the field \vec{E} can be related to the paraxial description \vec{E}_{inc} by evoking the assumption of aplanatic focusing, i.e., the sine condition is met, and energy is conserved [30,32]. In principle, the problem, then, is finding \vec{E} given \vec{E}_{inc} and computing the weighting coefficients, $g_{j,m_z}^{(m),(e)}$, given by the overlap integral of \vec{E} and the multipole fields. These integrals can be simplified by using the cylindrical symmetry of the input beam [20,31,32]. The tight focusing of SV beams can then be calculated from the addition of these fields using Eq. (3). These results are verified using the more common Debye-Wolf integral [30]. Several generated SV beam profiles at the focus of a $NA = 0.9$, $f = 1$ mm objective in free space are shown in [Fig. 3](#). Calculations assume an incident beam waist (w_0) such that $w_0 = f \cdot NA$, and a total power of 1 mW at the focus. The transverse and longitudinal E-fields are plotted separately, and the profiles agree well with past results [24].

In numerical simulations, we choose gold nanorod quadrupers as the test structures to demonstrate selective excitation of various plasmon modes belonging to different irreducible representations. We considered three different configurations of gold nanorods, as shown in [Figs. 4\(a\)-\(c\)](#): radial, azimuthal, and axial. All three of these structures possess the symmetry of the D_{4h} group. The focused SV beam generated by the method described above is imported as the source and placed at $z = -50$ nm for the radial and azimuthal quadrupers simulations, and at $z = -150$ nm for the axial quadrupers simulations. The beam is then allowed to propagate in the $+\hat{z}$ direction, forming a waist at the $z = 0$ plane where the center of each quadrupers is located. The optical constant of gold is taken from Johnson and Christy [34]. The incident SV beams,

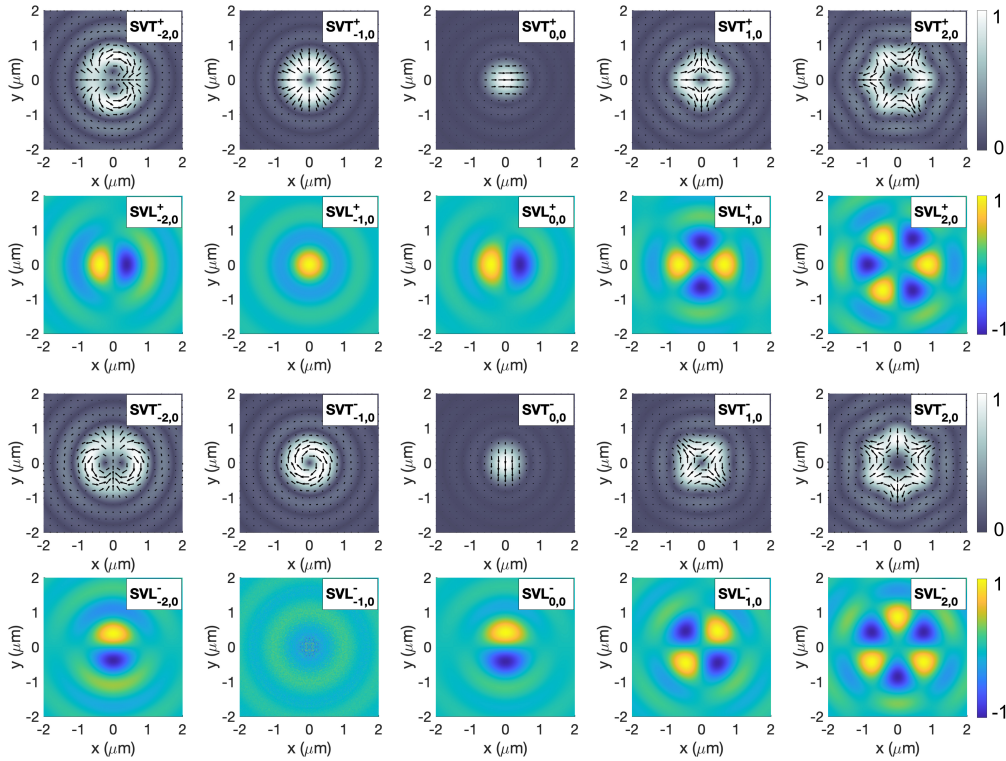


Fig. 3. The transverse and longitudinal E-field of a set of tightly focused SV beams on the focal plane. The wavelength is $1 \mu\text{m}$. The arrows in the 1st and 3rd rows represent the instantaneous \vec{E}_t vector, and the brightness corresponds to the normalized intensity $|\vec{E}_t|$ distribution. The color map in the 2nd and 4th rows represents the instantaneous \vec{E}_l value normalized by $|\vec{E}_l|_{\text{max}}$, in which yellow is positive and blue is negative. Because the tight focusing of azimuthally polarized beam $SV_{-1,0}^{-}$ results in no longitudinal E-field, the color map of $SVL_{-1,0}^{-}$ only represents the noise from numerical calculation error. As time evolves, the $SVT_{l,p}^{\alpha}$ fields simply oscillate in the transverse direction with the same polarization distribution and $SVL_{l,p}^{\alpha}$ fields simply oscillate in the longitudinal direction with the same amplitude distribution. (See also [Visualization 1](#) which shows the time evolution of a tightly focused $SV_{1,0}^{+}$ beam's electric vector field on focal plane.)

which are focused by a $NA = 0.9$, $f = 1 \text{ mm}$ objective in free space, are calculated for multiple wavelengths across $0.5 \sim 1.7 \mu\text{m}$ and the power is normalized to 1 mW at all wavelengths.

For each nanorod, the degeneracy between the longitudinal dipole resonance and the two transverse dipole resonances is lifted due to the asymmetry of the nanorod geometry. The high aspect ratio of the structure was chosen to closely reproduce the point group symmetry and isolate the eigenmodes from each other, while the dimensions ensure individual nanorod's longitudinal dipole resonances in the near-infrared region. Therefore, for the radial nanorod quadrumer, only the plasmon modes hybridized by radial dipole resonances will be excited in the visible and near-infrared region while the plasmon modes hybridized by azimuthal or axial dipole resonances are resonant at much shorter wavelengths. Now we can make linear combinations of the four E_u hybridized-dipole eigenmodes in Fig. 2 and obtain the radial x(y)-dipole mode and azimuthal x(y)-dipole mode as shown in Fig. 5. Each pair forms a basis function set for the E_u representation. For the radial nanorod quadrumer (Fig. 4(a)), the radial dipole modes will

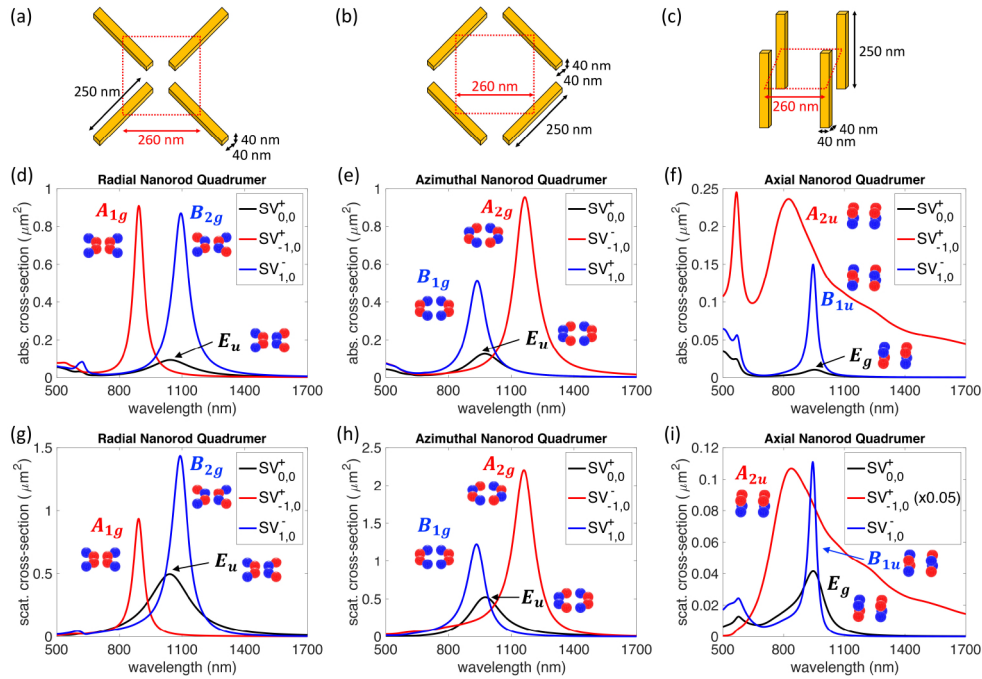


Fig. 4. (a-c) Illustration of the gold radial (azimuthal, axial) nanorod quadrupler. The quadrupler shares the same symmetry axis as the incident beam and the center of each nanorod is located at the beam’s focal plane. (d-f) Absorption cross-section of the radial (azimuthal, axial) nanorod quadrupler with tightly focused $SV_{0,0}^+$ (black line), $SV_{-1,0}^+$ (red line) and $SV_{1,0}^+$ (blue line) beams incident. Inset images are renderings of the quadrupler’s hybridized-dipole plasmon mode corresponding to each excitation peak. (g-i) Scattering cross-section of the radial (azimuthal, axial) nanorod quadrupler with tightly focused $SV_{0,0}^+$ (black line), $SV_{-1,0}^+$ (red line) and $SV_{1,0}^+$ (blue line) beams incident. In chart (i) the scattering cross-section of axial nanorod quadrupler with tightly focused $SV_{-1,0}^+$ beam incident (red line) has been multiplied by a factor of 0.05. (See also [Visualization 2](#) which shows the time evolution of the surface charge distribution of the B_{1g} mode excited by a tightly focused $SV_{1,0}^+$ beam.)

produce resonances in the visible and near-infrared region, but the azimuthal dipole modes will not. Similarly, for the azimuthal nanorod quadrupler (Fig. 4(b)), only the azimuthal dipole modes will exhibit resonances in the visible and near-infrared region.

	Radial dipole modes	Azimuthal dipole modes
Hybridized-dipole E_u plasmon mode		

Fig. 5. The symmetry-adapted hybridized-dipole eigenmodes that belong to the E_u representation. The radial x(y)-dipole mode is hybridized by only the radial dipole resonances of the nanorods, and the azimuthal x(y)-dipole mode is hybridized by only the azimuthal dipole resonances of the nanorods.

To demonstrate the selection rule based on the symmetry, we calculated the absorption and scattering spectra and the surface charge distribution for each coupling cases between the 3 quadrumers and 5 different tightly focused SV beams — $SV_{0,0}^+$, $SV_{-1,0}^\pm$ and $SV_{1,0}^\pm$. As shown in Figs. 4(d) and 4(g) for the radial nanorod quadrumer, a tightly focused $SV_{0,0}^+$ beam (x-polarized Gaussian beam) can only excite the radial x-dipole plasmon mode (E_u mode) but not the A_{1g} and B_{2g} plasmon modes which are orthogonal to the $SV_{0,0}^+$ beam. A tightly focused $SV_{-1,0}^+$ beam whose transverse component is a basis function of the A_{1g} representation only excites the A_{1g} plasmon mode. Finally, a tightly focused $SV_{1,0}^-$ beam whose transverse component is a basis function of the B_{2g} representation only excites the B_{2g} plasmon mode.

The selection rule is further confirmed by the spectra of azimuthal and axial nanorod quadrumers. As shown in Figs. 4(e) and 4(h), the azimuthal x-dipole plasmon mode (E_u mode) of the azimuthal nanorod quadrumer is excited only by a tightly focused $SV_{0,0}^+$ beam whose transverse component is a “x-type” basis function of the E_u representation. Similarly, a tightly focused $SV_{-1,0}^-$ beam whose transverse component is a basis function of the A_{2g} representation only excites the A_{2g} plasmon mode, and a tightly focused $SV_{1,0}^+$ beam whose transverse component is a basis function of the B_{1g} representation only excites the B_{1g} plasmon mode.

For the axial nanorod quadrumer, as shown in Figs. 4(f) and 4(i), only a tightly focused $SV_{-1,0}^+$ beam whose longitudinal component belongs to the A_{2u} representation couples to the bright out-of-plane dipole plasmon mode at normal incidence. A tightly focused $SV_{0,0}^+$ beam whose longitudinal component is a “x-type” basis function of the E_g representation only excite the “x-type” E_g quadrupole plasmon mode. And a tightly focused $SV_{1,0}^-$ beam whose longitudinal component is a basis function of the B_{1u} representation only excites the B_{1u} plasmon mode, which is an octupole mode.

These simulation results clearly show that the tightly focused SV beams selectively excite plasmon modes with specific symmetry as classified by the group representation theory. Note that SV beams form a complete, orthonormal basis for the solutions of paraxial wave equation. Thus, the selection rule can be applied to any cylindrical beam which is a solution to the paraxial wave equation by decomposing it into a linear combination of SV beams. For example, a circularly polarized Laguerre–Gaussian beam with azimuthal parameter $l = 1$ and radial parameter $p = 0$ and polarization handedness \hat{e}_+ can be written in terms of SV modes as

$$LG_{1,0}^+ = SV_{1,0}^+ + iSV_{1,0}^- . \quad (12)$$

According to Table 1, under tight focusing this beam is decomposed into $SV_{1,0}^+ + iSV_{1,0}^- + SV_{1,0}^+ + iSV_{1,0}^-$ which belong to the D_{4h} group’s irreducible representations B_{1g} , B_{2g} , B_{2u} and B_{1u} , respectively. Therefore, tightly focused $LG_{1,0}^+$ beam should only be able to couple into the plasmon modes belonging to these four representations.

To illustrate this point, we designed a radial nanorod octamer structure composed of 2 sets of radial nanorod quadrumers with different lengths, as shown in Fig. 6(a). This structure still has the D_{4h} symmetry, but because it is largely compressed in the vertical direction, only the in-plane hybridized-dipole plasmon modes (which are basis functions of the A_{1g} , A_{2g} , B_{1g} , B_{2g} , E_u representations) will exhibit resonance in the $0.5 \sim 1.7 \mu\text{m}$ wavelength range we studied. According to the calculated cross-section shown in Figs. 6(b) and 6(c), the $SV_{1,0}^+$ component can only excite the B_{1g} mode, and the $SV_{1,0}^-$ component can only excite the B_{2g} mode as expected from the selection rule. Meanwhile, the $LG_{1,0}^+$ beam, which is a combination of both $SV_{1,0}^+$ and $SV_{1,0}^-$, excites both plasmon modes. This example clearly shows the fundamental advantage of using SV beams as the incident beams for selective excitation compared to Laguerre–Gaussian beams. Specifically, the SV beams have one-to-one selectivity derived from their symmetry properties, but the Laguerre–Gaussian beams do not.

It is noted that, although the $SV_{1,0}^+$ and $SV_{1,0}^-$ beams are identical except for their azimuthal orientations, they excite plasmon modes with distinct symmetry. This result shows that the

azimuthal orientation of the SV beam must match that of the nanostructure in order to achieve selective excitation. In general, we can build a Cartesian coordinate system based on the nanostructure's axial symmetry axis (z -axis) and its secondary symmetry axis (x -axis) to specify the azimuthal orientation of $SV_{l,p}^{\pm}$ beams. Any azimuthally misaligned SV beam can then be written as a linear combination of the $SV_{l,p}^{\pm}$ basis:

$$\hat{P}_{R_z(\theta)}SV_{l,p}^{\pm} = \cos\theta \cdot SV_{l,p}^{\pm} \mp \sin\theta \cdot SV_{l,p}^{\mp} . \quad (13)$$

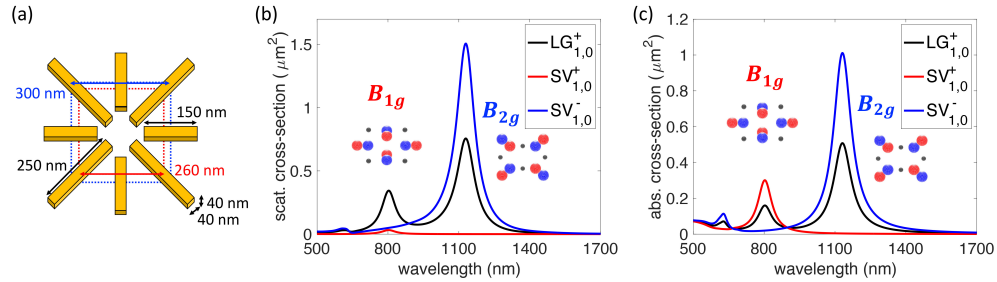


Fig. 6. (a) Illustration of the gold radial nanorod octamer structure composed of 2 sets of radial nanorod quadrumers with different lengths. (b) Absorption cross-section of the octamer with tightly focused $LG_{1,0}^+$ (black line), $SV_{1,0}^+$ (red line) and $SV_{1,0}^-$ (blue line) beams excitation. Inset images are renderings of the symmetry-adapted hybridized-dipole B_{1g} and B_{2g} modes of the nanorod octamer. (c) Scattering cross-section of the octamer with tightly focused $LG_{1,0}^+$ (black line), $SV_{1,0}^+$ (red line) and $SV_{1,0}^-$ (blue line) beams excitation.

It can be treated as having both $SV_{l,p}^{\pm}$ components, each of which follows the selection rule described above.

So far, we have only considered nanostructures embedded in a homogenous medium. In these cases, the symmetry of both the plasmon modes and SV beams is described by the same point group, D_{nh} , leading to a straightforward selection rule as described above. If, however, the nanostructure is placed on a substrate, or if the nanostructure is not placed exactly at the incident beam's focal plane, the horizontal mirror symmetry is destroyed, and the symmetry properties are no longer described by a D_{nh} point group. In these cases, since the incident beam and the plasmonic structure still share the same axis of symmetry, we can always find a subgroup of D_{nh} to describe the plasmonic structure's symmetry. Since the basis functions of D_{nh} groups are also the basis functions of their subgroups, e.g., D_n , C_{nh} , C_n groups, we can still use the SV beams to decompose the incident beam and construct a correlation table similar to Table 1 for these subgroups by applying the same selection rule.

Another situation to consider is the oblique incidence, where the incident beam and plasmonic structure have the same center of symmetry but there is an angular misalignment between their symmetry axes. In the near-field region of the plasmonic structure, we can decompose the incident field into a linear combination of a normal incidence component and a perpendicular incidence component. Both components have the same field pattern as the original beam but are scaled in amplitude. The normal component will be subject to the same selection rule we discussed earlier. For the perpendicular component, one needs to perform a separate mode overlap calculation, because the plasmonic nanostructure does not exhibit a well-defined axial symmetry for the incident light coming from the side.

4. Conclusion

In conclusion, we have introduced a new framework for understanding the excitation of localized surface plasmon resonances with cylindrical vector beams via symmetry coupling. The SV beams have intrinsic reflection symmetries that make them a much more suitable basis for symmetry analysis than the commonly used circularly polarized Laguerre–Gaussian beam basis. We utilized the orthogonality of the SV beams and plasmon resonances naturally arising from their symmetry properties and clearly elucidated by the group theory analysis to derive the selection rules for the excitation without conducting any numerical simulations or overlap integral calculations. We identified and demonstrated that SV beams have one-to-one correspondence with the plasmon modes in axially symmetric nanostructures, thereby enabling truly selective excitation of any mode supported by the nanostructure. Second, the SV beams allow selective excitation even in the case of tight focusing, which is often needed for efficient coupling with nanostructures. A tightly focused SV beam can be decomposed into transverse and longitudinal components, each of which maintains one-to-one correspondence with the plasmon modes.

In this framework, to selectively excite a particular plasmon eigenmode, all we need is to find which SV beams (or beam components) belong to the same irreducible representation as the desired plasmon mode. With the possibility of synthesizing SV beams using, for example, a spatial light modulator [35,36], we believe our work provides a plausible path toward experimentally demonstrating selective excitation of any arbitrary plasmon mode with a tightly focused beam. We showed that any cylindrical beam can be decomposed into a series of SV beams and by identifying the SV beams included in the decomposition, one can determine which plasmon modes would be excited. Therefore, our framework can not only explain the selective excitation phenomena, but also guide the design of nanostructures and choice of incident beams to excite desired resonance modes individually or jointly without extensive numerical calculations.

Although we limited our discussion to plasmon modes in this paper, it is straightforward to apply the same theory to the localized resonances supported by dielectric nanostructures since the symmetry arguments are agnostic to the choice of materials. The group theory guided symmetry coupling method can be a powerful tool for exploring dark modes or higher order modes which are generally difficult to excite using conventional Gaussian beams. With full access to the localized resonances in a nanostructure, one may envision a wide range of photonic engineering that exploits the precise control of the plasmonic near-field by combining or switching between the individual multipole modes even when they spectrally overlap. This framework also opens the opportunity to realize strong coupling between electronic excitations in localized emitters and dark plasmons which can be the platform to develop novel non-linear plasmonic devices.

Funding. National Science Foundation (DGE 1650115, DMR 1553905, ECCS 1554704).

Acknowledgments. We gratefully acknowledge useful technical discussions with Gabriel Molina-Terriza.

Disclosures. The authors declare no conflict of interest.

Data Availability. Data underlying the results presented in this paper are not publicly available at this time but may be obtained from the authors upon reasonable request.

Supplemental document. See [Supplement 1](#) for supporting content.

References

1. M. Li, S. K. Cushing, and N. Wu, "Plasmon-enhanced optical sensors: a review," *Analyst* **140**(2), 386–406 (2015).
2. K. Aslan, J. R. Lakowicz, and C. D. Geddes, "Plasmon light scattering in biology and medicine: new sensing approaches, visions and perspectives," *Curr. Opin. Chem. Biol.* **9**(5), 538–544 (2005).
3. E. Fort and S. Grésillon, "Surface enhanced fluorescence," *J. Phys. D: Appl. Phys.* **41**(1), 013001 (2007).
4. M. K. Hossain, Y. Kitahama, G. G. Huang, X. Han, and Y. Ozaki, "Surface-enhanced Raman scattering: realization of localized surface plasmon resonance using unique substrates and methods," *Anal. Bioanal. Chem.* **394**(7), 1747–1760 (2009).
5. C. Hubert, L. Billot, P.-M. Adam, R. Bachelot, P. Royer, J. Grand, D. Gindre, K. Dorkenoo, and A. Fort, "Role of surface plasmon in second harmonic generation from gold nanorods," *Appl. Phys. Lett.* **90**(18), 181105 (2007).

6. L. Qiao, D. Wang, L. Zuo, Y. Ye, J. Qian, H. Chen, and S. He, "Localized surface plasmon resonance enhanced organic solar cell with gold nanospheres," *Appl. Energy* **88**(3), 848–852 (2011).
7. S. Ahn, D. Rourke, and W. Park, "Plasmonic nanostructures for organic photovoltaic devices," *J. Opt.* **18**(3), 033001 (2016).
8. K. Awazu, M. Fujimaki, C. Rockstuhl, J. Tominaga, H. Murakami, Y. Ohki, N. Yoshida, and T. Watanabe, "A plasmonic photocatalyst consisting of silver nanoparticles embedded in titanium dioxide," *J. Am. Chem. Soc.* **130**(5), 1676–1680 (2008).
9. D. Gómez, Z. Teo, M. Altissimo, T. Davis, S. Earl, and A. Roberts, "The dark side of plasmonics," *Nano Lett.* **13**(8), 3722–3728 (2013).
10. N. A. Mirin, K. Bao, and P. Nordlander, "Fano resonances in plasmonic nanoparticle aggregates," *J. Phys. Chem. A* **113**(16), 4028–4034 (2009).
11. J. Sancho-Parramon and S. Bosch, "Dark modes and Fano resonances in plasmonic clusters excited by cylindrical vector beams," *ACS Nano* **6**(9), 8415–8423 (2012).
12. T.-S. Deng, J. Parker, Y. Yifat, N. Shepherd, and N. F. Scherer, "Dark plasmon modes in symmetric gold nanoparticle dimers illuminated by focused cylindrical vector beams," *J. Phys. Chem. C* **122**(48), 27662–27672 (2018).
13. F. Xiao, W. Shang, W. Zhu, L. Han, M. Premaratne, T. Mei, and J. Zhao, "Cylindrical vector beam-excited frequency-tunable second harmonic generation in a plasmonic octamer," *Photonics Res.* **6**(3), 157–161 (2018).
14. F. Xiao, G. Wang, X. Gan, W. Shang, S. Cao, W. Zhu, T. Mei, M. Premaratne, and J. Zhao, "Selective excitation of a three-dimensionally oriented single plasmonic dipole," *Photonics Res.* **7**(6), 693–698 (2019).
15. K. Sakai, K. Nomura, T. Yamamoto, and K. Sasaki, "Excitation of multipole plasmons by optical vortex beams," *Sci. Rep.* **5**(1), 1–4 (2015).
16. I. A. Litvin, N. S. Mueller, and S. Reich, "Selective excitation of localized surface plasmons by structured light," *Opt. Express* **28**(16), 24262–24274 (2020).
17. T. Arikawa, S. Morimoto, and K. Tanaka, "Focusing light with orbital angular momentum by circular array antenna," *Opt. Express* **25**(12), 13728–13735 (2017).
18. R. M. Kerber, J. M. Fitzgerald, D. E. Reiter, S. S. Oh, and O. Hess, "Reading the orbital angular momentum of light using plasmonic nanoantennas," *ACS Photonics* **4**(4), 891–896 (2017).
19. R. W. Heeres and V. Zwiller, "Subwavelength focusing of light with orbital angular momentum," *Nano Lett.* **14**(8), 4598–4601 (2014).
20. X. Zambrana-Puyalto and G. Molina-Terriza, "The role of the angular momentum of light in Mie scattering. Excitation of dielectric spheres with Laguerre–Gaussian modes," *J. Quant. Spectrosc. Radiat. Transf.* **126**, 50–55 (2013).
21. E. J. Galvez, S. Khadka, W. H. Schubert, and S. Nomoto, "Poincaré-beam patterns produced by nonseparable superpositions of Laguerre–Gauss and polarization modes of light," *Appl. Opt.* **51**(15), 2925–2934 (2012).
22. A. M. Beckley, T. G. Brown, and M. A. Alonso, "Full Poincaré beams," *Opt. Express* **18**(10), 10777–10785 (2010).
23. C. Rosales-Guzmán, B. Ndagano, and A. Forbes, "A review of complex vector light fields and their applications," *J. Opt.* **20**(12), 123001 (2018).
24. E. Otte, K. Tekce, and C. Denz, "Tailored intensity landscapes by tight focusing of singular vector beams," *Opt. Express* **25**(17), 20194–20201 (2017).
25. D. W. Brandl, N. A. Mirin, and P. Nordlander, "Plasmon modes of nanosphere trimers and quadrumers," *J. Phys. Chem. B* **110**(25), 12302–12310 (2006).
26. D. Gómez, K. Vernon, and T. Davis, "Symmetry effects on the optical coupling between plasmonic nanoparticles with applications to hierarchical structures," *Phys. Rev. B* **81**(7), 075414 (2010).
27. M. S. Dresselhaus, G. Dresselhaus, and A. Jorio, *Group theory: application to the physics of condensed matter* (Springer Science & Business Media, 2007).
28. Q. Zhan, "Cylindrical vector beams: from mathematical concepts to applications," *Adv. Opt. Photonics* **1**(1), 1–57 (2009).
29. I. Freund, "Polarization singularity indices in gaussian laser beams," *Opt. Commun.* **201**(4–6), 251–270 (2002).
30. L. Novotny and B. Hecht, *Principles of nano-optics* (Cambridge University, 2012).
31. G. Molina-Terriza, "Determination of the total angular momentum of a paraxial beam," *Phys. Rev. A* **78**(5), 053819 (2008).
32. X. Zambrana-Puyalto, X. Vidal, and G. Molina-Terriza, "Excitation of single multipolar modes with engineered cylindrically symmetric fields," *Opt. Express* **20**(22), 24536–24544 (2012).
33. T. Nieminen, H. Rubinsztein-Dunlop, and N. Heckenberg, "Multipole expansion of strongly focused laser beams," *J. Quant. Spectrosc. Radiat. Transf.* **79–80**, 1005–1017 (2003).
34. P. B. Johnson and R.-W. Christy, "Optical constants of the noble metals," *Phys. Rev. B* **6**(12), 4370–4379 (1972).
35. D. Mao, Y. Zheng, C. Zeng, H. Lu, C. Wang, H. Zhang, W. Zhang, T. Mei, and J. Zhao, "Generation of polarization and phase singular beams in fibers and fiber lasers," *Adv. Photon.* **3**(01), 014002 (2021).
36. J. Liu, X. Chen, Y. He, L. Lu, H. Ye, G. Chai, S. Chen, and D. Fan, "Generation of arbitrary cylindrical vector vortex beams with cross-polarized modulation," *Results Phys.* **19**, 103455 (2020).